Magnetic Bloch oscillations in a non-Hermitian quantum Ising chain

K. L. Zhang and Z. Song[*]

School of Physics, Nankai University, Tianjin 300071, China

We investigate the impacts of an imaginary transverse field on the dynamics of magnetic domain walls in a quantum Ising chain. We show that an imaginary field plays a similar role as a real transverse field in forming a low-lying Wannier-Stark ladder. However, analytical and numerical calculations of the time evolutions in both systems show that the corresponding Bloch oscillations exhibit totally different patterns for the same initial states. These findings reveal the nontrivial effect of non-Hermiticity on quantum spin dynamics.

I. INTRODUCTION

Bloch oscillation (BO) describes the periodic motion of a wave packet subjected to an external force in a lattice. This phenomenon was first noted by Bloch and Zener when they studied the electrical properties of crystals [1,2]. When an external electric field is applied to a perfect crystal lattice, the localized eigenstates with a ladderlike energy spectrum emerge, known as the Wannier-Stark (WS) ladder [3]. These states are closely related to the BOs, which can be understood as the periodic motion of a wave packet within the WS ladder, as an external field causes the wave packet to transition between different WS states and exhibit oscillatory behavior in terms of position and velocity. Experimentally, BOs were observed in a semiconductor superlattice [4], ultracold atoms in the optical lattice [5–8], and many other systems sequentially [9–13]. It turns out that BO is a universal wave phenomenon. In the magnetic systems, BOs appear in the form of the magnetic domain-wall oscillations. As a nonequilibrium dynamic phenomenon in quantum many-body systems, magnetic BOs in the quantum spin chains have attracted much attention from researchers [13–21]. Notably, inelastic neutron-scattering experiments have provided evidence for the existence of magnetic BOs in the magnetically identical material $CoCl_2 2D_2O$ [13].

In recent years, non-Hermitian physics have attracted much attention from various research areas [22–33], and BOs have been investigated in a range of non-Hermitian systems, including photonic lattices with gain or loss [22,34,35], tight-binding chains with an imaginary gauge field [36–38], and non-Hermitian frequency lattices induced by complex photonic gauge fields [26]. Classical systems such as photonics, mechanics, and electrical circuits can be used to simulate non-Hermitian wave physics at the single-particle level, while in the quantum systems non-Hermitian Hamiltonians are mainly explained as the effective descriptions of open quantum systems [27], and have been experimentally realized in the systems of superconducting quantum circuits [39,40],

nitrogen-vacancy centers in diamonds [29,41], and ultracold atoms [42,43]. Moreover, it was proposed that an imaginary field in a spin chain can be implemented by a scheme similar to heralded entanglement protocols [24]. More recently, researchers have shown that complex fields in quantum spin models have unique impacts on the physical properties of the systems [44–53], for example, by driving a quantum phase transition and altering the phase diagram of the system. However, to the best of our knowledge, the BO in a non-Hermitian quantum spin chain has not yet been explored.

In this paper, we investigate the BOs of magnetic domain walls in a non-Hermitian quantum Ising chain. The model considered is a quantum Ising chain with real longitudinal and imaginary transverse fields. We show that in the small-field region, i.e., when the strengths of two fields are much smaller than the Ising coupling, as well as in the $\mathcal{PT}$-symmetric parameters region that guarantees a full real spectrum, the low-energy dynamics of the magnetic domain walls are captured by a single-particle effective Hamiltonian, through which the physical mechanism of magnetic BOs is revealed. For real and imaginary transverse fields, the eigenstates of the effective Hamiltonian are both localized states with ladderlike energy spectra, forming the WS ladders. Analytical analysis and numerical calculation of the time evolutions show the occurrence of magnetic breathing and BO modes in the non-Hermitian quantum Ising chain by appropriately selecting the initial states. It is shown that for the non-Hermitian quantum Ising chain, the dynamics for the Kronecker delta initial state is a breathing mode, while the Gaussian state remains stationary, which is totally different from the oscillation of the domain wall in a Hermitian quantum Ising chain. Interestingly, for the Bessel initial state, the BO mode appears, and the amplitude can be modulated by the strength of the imaginary transverse field and the localization length of the initial state.

This paper is organized as follows. In Sec. II, we start by introducing the Hamiltonian of the quantum Ising chain with an imaginary transverse field, and derive the effective Hamiltonian and its solution. In Sec. III, we analyze the dynamics of BOs for three types of initial states on the basis of the effective Hamiltonian, while Sec. IV presents the numerical results of

*songtc@nankai.edu.cn

the dynamics for the quantum spin chain. Finally, we conclude our findings in Sec. V.

II. MODEL AND EFFECTIVE HAMILTONIAN

The model we consider is a quantum spin chain of length N with the Hamiltonian

$$H = H_0 + H', \tag{1}$$

where

$$H_0 = -J \sum_{j=1}^{N-1} \sigma_j^z \sigma_{j+1}^z - h_z \sum_{j=1}^{N} \sigma_j^z \tag{2}$$

represents a spin chain in longitudinal magnetic field $-h_z$, and with ferromagnetic Ising coupling $-J$. For simplicity, we set $J = 1$ in the following discussion. Here σ_j^α ($\alpha = x, y, z$) are the Pauli operators on site j, while

$$H' = -g \sum_{j=1}^{N} \sigma_j^x \tag{3}$$

is a transverse magnetic field term. In this paper, we consider both the Hermitian and non-Hermitian systems, when the transverse fields g are taken as real and imaginary, respectively. We would like to point out that the Hamiltonian H is different from that of the Yang-Lee Ising spin model, which exhibits Lee-Yang zeros [54–60]; in this model, the longitudinal field is imaginary, and the transverse field is real instead. When $h_z = 0$, the Hamiltonian H reduces to the transverse field Ising chain, which is exactly solvable through the Jordan-Wigner transformation when the periodic boundary condition is applied, and serves as a unique paradigm for understanding the quantum phase transition [61]. A nonzero longitudinal field term involves nonlocal operators in the fermion representation, and thus breaks the solvability of the model.

Imaginary fields in quantum spin systems have been discussed in many experimental and theoretical works [24,29,41–43,62–64]. In the framework of open quantum system dynamics, the imaginary transverse field g arises in the no-click limit of the stochastic quantum jump trajectories when $(1 + \sigma_j^x)/2$ is measured [62–64], and $|g|$ can be interpreted as either dissipation or measurement rate. In this case, the resulted non-Hermitian Hamiltonian H respects $\mathcal{PT}$ symmetry, that is, $[\mathcal{PT}, H] = 0$, with $\mathcal{P} = \prod_{j=1}^{N} \sigma_j^z$ being the parity operator, and $\mathcal{T}$ being the complex conjugation operator. This guarantees a full real spectrum in a certain region of system parameters [57,65–67], which is the so-called $\mathcal{PT}$-symmetric region where the eigenstates remain unchanged under the action of the $\mathcal{PT}$ operator. Beyond this region, the eigenvalues occur in complex conjugate pairs and the corresponding eigenstates change under the action of the $\mathcal{PT}$ operator. Due to the lack of solvability in the model, the phase boundary of these two regions cannot be obtained analytically. Nevertheless, it is expected that the system possesses a full real spectrum when $|g|$ is small compared to other system parameters. In Fig. 1, we presented the numerical result of the phase diagram of broken and unbroken $\mathcal{PT}$ symmetry for a finite-size system. The $\mathcal{PT}$-symmetric region is determined
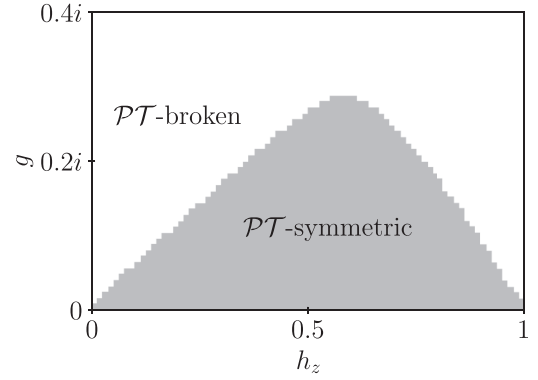

FIG. 1. Schematic of $\mathcal{PT}$-symmetric (gray) and $\mathcal{PT}$-broken (white) regions in the h_z-g plane. The result is obtained by numerical exact diagonalization for a Hamiltonian H with $J = 1$ and $N = 10$.

by condition $\sum_{n=1}^{2^N} |\text{Im}(\varepsilon_n)|/2^N < 0.01$, where ε_n is the energy level of system H.

In this paper, we are concerned with the dynamics in the low-energy subspace as well as in the $\mathcal{PT}$-symmetric parameters region of the model. Thus, we content ourselves with a perturbation solution through seeking for an effective Hamiltonian describing the low-energy dynamics. To proceed, we concentrate on the weak-field situation with $h_z, |g| \ll J$, and treat the transverse field term H' as a perturbation in the following discussion.

We note that all the eigenstates of H_0 can be written in the tensor product form with fixed numbers of spins that are parallel or antiparallel to the z direction. The ground state of H_0 is $|\Uparrow\rangle = \prod_{j=1}^{N} |\uparrow\rangle_j$ with energy $\mathcal{E}_G = -N(J + h_z) + J$. We focus on the low-energy subspace $\{|\phi_m^\pm\rangle\}$ that consists of states having one magnetic domain wall. Here $|\phi_m^\pm\rangle$ represent two types of domain-wall states:

$$|\phi_m^+\rangle = \prod_{l \leqslant m} \sigma_l^- |\Uparrow\rangle, \quad |\phi_m^-\rangle = \prod_{l > m} \sigma_l^- |\Uparrow\rangle, \tag{4}$$

with $\sigma_j^- = (\sigma_j^x - i\sigma_j^y)/2$ the lowering operator, and $m = 1, 2, \ldots, N-1$ the spatial position of the domain wall. The corresponding energy is $\mathcal{E}_m^\pm = -N(J \pm h_z) + 3J \pm 2mh_z$. The action of H on this basis yields

$$H|\phi_m^\pm\rangle = [-N(J \pm h_z) + 3J \pm 2mh_z]|\phi_m^\pm\rangle$$
$$- g|\phi_{m+1}^\pm\rangle - g|\phi_{m-1}^\pm\rangle - g(\ldots). \tag{5}$$

Here the ellipsis dots "..." represent the terms containing the basis states with more than one domain wall, which have at least $2J$ energy difference compared to the states in $\{|\phi_m^\pm\rangle\}$. Thus, we are able to adiabatically eliminate these states and project the Hamiltonian H into the subspace $\{|\phi_m^\pm\rangle\}$. The effective Hamiltonian is given by [68]

$$H_{\text{eff}} = PHP - PHQ \frac{1}{QHQ} QHP, \tag{6}$$

where the projectors are defined as $P = \sum_{m,\pm} |\phi_m^\pm\rangle\langle\phi_m^\pm|$ and $Q = 1 - P$. The second term in Eq. (6) that is proportional to g^2 is discarded, considering the solvability of the effective Hamiltonian, and $|g|$ is a small quantity. Up to first order, the

effective Hamiltonian has the explicit form

$$
H_{\text{eff}} = -g \sum_{\lambda=\pm} \sum_{m=1}^{N-2} \left(|\phi_m^\lambda\rangle\langle\phi_{m+1}^\lambda| + |\phi_{m+1}^\lambda\rangle\langle\phi_m^\lambda| \right)
$$
$$
+ \sum_{\lambda=\pm} \sum_{m=1}^{N-1} [-N(J+\lambda h_z) + 3J + 2\lambda m h_z] |\phi_m^\lambda\rangle\langle\phi_m^\lambda|.
$$
$$(7)$$

This indicates that the transverse field $-g$ acts as a hopping coefficient for the magnetic domain wall, while the strength of the longitudinal field h_z plays the role of a skew potential. Next, we investigate the dynamics in $\{|\phi_m^+\rangle\}$ subspace, and denote $|\phi_m\rangle = |\phi_m^+\rangle$ for simplicity. The analysis is similar for that of $\{|\phi_m^-\rangle\}$ subspace. In the absence of the skew potential h_z, the k-periodic spectrum is $E(k) = -2g\cos(k) +$ const for the Bloch wave of magnetic excitation $|\phi(k)\rangle = (2\pi)^{-1/2} \sum_m e^{imk} |\phi_m\rangle$. For a real g, the semiclassical picture of BOs has been well understood [1,2]. However, for an imaginary g, the semiclassical picture should be understood in the framework of a modified equation of motion for expectation values, and the acceleration theorem holds only on average in time [37,38].

The eigenstate of the Hamiltonian H_{eff} can be expanded as $|\psi_n\rangle = \sum_m C_m^{(n)} |\phi_m\rangle$, and the stationary Schrödinger equation $H_{\text{eff}} |\psi_n\rangle = E_n |\psi_n\rangle$ gives the recursive relation for the expansion coefficients:

$$
C_{m+1}^{(n)} + C_{m-1}^{(n)} = \frac{2\alpha_m}{z} C_m^{(n)}, \tag{8}
$$

with $\alpha_m = (3J - NJ - E_n)/(2h_z) + m - N/2$ and $z = g/h_z$. The boundary condition is $C_0^{(n)} = C_N^{(n)} = 0$. We identify that Eq. (8) is the recursive formula of the Bessel function. Since the boundary effect is not involved in the dynamics that we will investigate in the next section, we assume an infinite chain in the following analytical analysis for convenience. Then the solution can be written as

$$
C_m^{(n)} = J_{m-n}(z), \tag{9}
$$

which is the Bessel function of the first kind. Notably, the argument z is imaginary for a non-Hermitian system. These eigenstates can be related by the spatial translation operation, that is, $\mathcal{T}|\psi_n\rangle = |\psi_{n+1}\rangle$ with the translation operator $\mathcal{T}$ defined as $\mathcal{T}|\phi_m\rangle = |\phi_{m+1}\rangle$. Then the eigenstates for the Hamiltonian H_{eff} are

$$
|\psi_n\rangle = \sum_m J_{m-n}(z) |\phi_m\rangle, \tag{10}
$$

with energy $E_n = -N(J+h_z) + 3J + 2nh_z$, which is equally spaced and independent of g.

Similarly, the eigenstate of the Hamiltonian $H_{\text{eff}}^\dagger$ with energy E_n is

$$
|\varphi_n\rangle = \sum_m J_{m-n}(z^*) |\phi_m\rangle, \tag{11}
$$

which establishes a biorthonormal basis set satisfying

$$
\langle\varphi_{n'}|\psi_n\rangle = \delta_{n',n}, \tag{12}
$$

$$
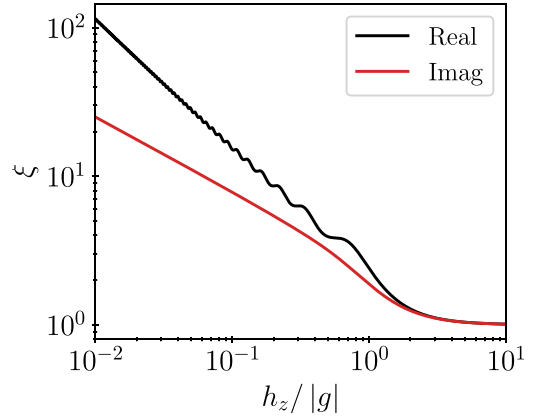\sum_n |\psi_n\rangle\langle\varphi_n| = 1. \tag{13}
$$

FIG. 2. Numerical results of the localization length ξ defined in Eq. (14) as a function of h_z (in units of $|g|$). The black and red lines represent the data for the real g and imaginary g, respectively. The horizontal and vertical axes are both on a logarithmic scale. The other parameters are set as $N = 10^4$, $J = 1$, and $n = N/2$.

It is well known that the eigenstates are localized for a Hermitian WS ladder [69]. Thus, it can be reasonably inferred that this is also the case for an imaginary g. This can be confirmed by the localization length for the eigenstate, which is defined as [19,70]

$$
\xi = \frac{\left[\sum_m |J_{m-n}(z)|^2\right]^2}{\sum_m |J_{m-n}(z)|^4}. \tag{14}
$$

For an infinite system, ξ is independent of energy. Also, ξ of the localized state is independent of N when N is large enough. In Fig. 2, we present the numerical results of the localization length ξ of the eigenstates for the real and imaginary fields g, respectively. We can see that for both cases, a nonzero longitudinal h_z field induces the localization of the eigenstates, which is more pronounced for an imaginary g. The localization of eigenstates is crucial for the upcoming discussion.

III. ANALYSES FOR THE OSCILLATION DYNAMICS

In this section, we investigate the dynamics of magnetic BOs in a non-Hermitian quantum spin chain through an analytical analysis of the effective Hamiltonian. The characteristics of eigenstate localization and equal spacing of energy levels are both crucial for the construction of the initial excitation of the magnetic BOs.

We consider the initial states

$$
|\Psi(0)\rangle = \sum_m f_m(0) \prod_{l \leqslant m} \sigma_l^- |\Uparrow\rangle = \sum_m f_m(0) |\phi_m\rangle \tag{15}
$$

with three types of distributions representing the domain wall localized at site m_0: (i) the delta function $f_m^{(1)}(0) = \delta_{m,m_0}$; (ii) the broad Gaussian distribution $f_m^{(2)}(0) = \mathcal{N}^{-1} e^{-\alpha^2(m-m_0)^2 + ik_0 m}$ where $\mathcal{N}$ is a normalization coefficient, α characterizes the width of the distribution, and k_0 is the wave vector; and (iii) the Bessel distribution $f_m^{(3)}(0) = \Omega^{-1} J_{m_0-m}(\kappa)$ with a complex argument κ. According to the Schrödinger equation, the evolved state can be formally

written as

$$|\Psi(t)\rangle = \sum_m f_m(t)|\phi_m\rangle$$

$$= \sum_{m,m'} K_{m,m'}(t) f_{m'}(0)|\phi_m\rangle. \tag{16}$$

From the solution in Eqs. (10)–(13), the propagator $K_{m,m'}(t)$ under the biorthonormal basis can be computed as follows:

$$K_{m,m'}(t) = \sum_n e^{-iE_n t} \langle m|\psi_n\rangle\langle\varphi_n|m'\rangle$$

$$= \sum_n e^{-iE_n t} J_{m-n}(z) J_{m'-n}^*(z^*), \tag{17}$$

and then using Graf's addition theorem [71,72] for the Bessel functions in the summation of index n, we arrive at

$$K_{m,m'}(t) = e^{i(\pi/2 - h_z t)(m-m') - i2m'h_z t} J_{m-m'}\left[\frac{2g\sin(h_z t)}{h_z}\right]. \tag{18}$$

Here, a m, m'-independent overall phase factor is discarded. Obviously, the propagator is periodic with a Bloch period $T = \pi/h_z$.

A. Kronecker delta initial state

Then, for the initial state $f_m^{(1)}(0) = \delta_{m,m_0}$, the evolved state is simply

$$f_m^{(1)}(t) = \sum_{m'} K_{m,m'}(t)\delta_{m',m_0}$$

$$= e^{i(\pi/2 - h_z t)(m-m_0) - i2m_0 h_z t} J_{m-m_0}\left[\frac{2g\sin(h_z t)}{h_z}\right]. \tag{19}$$

According to the properties of Bessel functions, the width of the domain wall periodically widens and narrows within the range

$$|m - m_0| \lesssim \left|\frac{2g\sin(h_z t)}{h_z}\right|, \tag{20}$$

for both real and imaginary field g with period $T = \pi/h_z$, which is the Bloch breathing mode. The profile of the evolved state here is independent of the particular value of initial position m_0.

B. Gaussian initial state

The evaluation of the time evolution for the initial state with Gaussian distribution is not straightforward. Some approximations are needed. To do this, we first Fourier transform the time-evolution equation $f_m^{(2)}(t) = \sum_{m'} K_{m,m'}(t)f_{m'}^{(2)}(0)$ into k space:

$$f_k^{(2)}(t) = \mathcal{N}^{-1}\sum_{m,m'} e^{-ikm}K_{m,m'}(t)e^{-\alpha^2(m'-m_0)^2 + ik_0 m'}$$

$$= \mathcal{N}^{-1}\exp\left[\frac{2gi\sin(h_z t)\cos(h_z t + k)}{h_z}\right]$$

$$\times \sum_{m'} e^{-\alpha^2(m'-m_0)^2 - i(k-k_0 + 2h_z t)m'}. \tag{21}$$

Assume that the spatial localization of the initial distribution is weak, that is, $\alpha \ll 1$, so that the summation of m' can be approximately replaced by integration. By doing this, we achieve

$$f_k^{(2)}(t) \approx \frac{\sqrt{\pi}}{\alpha}\mathcal{N}^{-1}\exp\left[\frac{2gi\sin(h_z t)\cos(h_z t + k)}{h_z}\right]$$

$$\times e^{-i(k-k_0 + 2h_z t)m_0}\exp\left[-\frac{(k - k_0 + 2h_z t)^2}{4\alpha^2}\right]. \tag{22}$$

Again, since $\alpha \ll 1$ is assumed, the momentum distribution $f_k(t)$ is sharply localized around $k_0 - 2h_z t$. Then, we can expand the factor $\cos(h_z t + k)$ in the argument of the exponential around $k_0 - 2h_z t$ up to the first order, and the evolved state in real space can be obtained as

$$f_m^{(2)}(t) = \frac{1}{2\pi}\int_{-\pi}^{\pi} e^{ikm}f_k(t)dk$$

$$\approx \mathcal{N}^{-1}\exp\{i(k_0 - 2h_z t)m - i\Phi(t) - \alpha^2[m - M(t)]^2\}, \tag{23}$$

where

$$\Phi(t) = \frac{g}{h_z}[\sin(k_0 - 2h_z t) - \sin k_0], \tag{24}$$

$$M(t) = m_0 + \frac{g}{h_z}[\cos(k_0 - 2h_z t) - \cos k_0]. \tag{25}$$

For a real g, the center of the wave packet $M(t)$ in real space oscillates in the form of a cosine function with period π/h_z and amplitude g/h_z, which is the BO mode. However, for an imaginary g, the center of the wave packet remains stationary at the initial position m_0 for any initial wave vector k_0. Thus, in the following, we seek for a new initial excitation enabling magnetic BO to occur in the non-Hermitian quantum Ising chain.

C. Bessel initial state

Finally, we compute the time evolution for the initial Bessel distribution $f_m^{(3)}(0) = \Omega^{-1}J_{m_0-m}(\kappa)$ where κ is a complex number characterizing the width of the initial distribution. Expanding this initial state with the biorthonormal basis, the superposition coefficient is

$$\langle\varphi_n|\Psi(0)\rangle = \Omega^{-1}J_{m_0-n}(\kappa + g/h_z). \tag{26}$$

For simplicity, we take $\kappa = x - g/h_z$ with a real x, then the above coefficient $\langle\varphi_n|\Psi(0)\rangle$ is always real. The time evolution is computed as

$$f_m^{(3)}(t) = \Omega^{-1}\sum_{m'} K_{m,m'}(t)J_{m_0-m'}(x - g/h_z)$$

$$= \Omega^{-1}e^{-i2mh_z t}\left(\frac{x - ze^{-2ih_z t}}{x - ze^{2ih_z t}}\right)^{(m_0-m)/2}$$

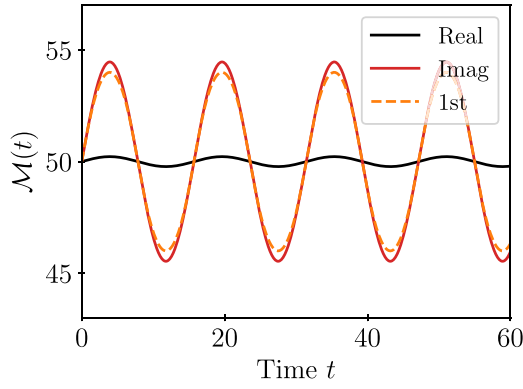$$\times J_{m_0-m}[\sqrt{x^2 + z^2 - 2xz\cos(2h_z t)}], \tag{27}$$

FIG. 3. Numerical results of the center of the wave packet as a function of time defined in Eq. (29) for different fields: $g = 0.1$ and $0.1i$ for the black and red lines, respectively. In addition, the orange dashed line represents the data obtained from Eq. (28) with a first-order approximation for the case of $g = 0.1i$. A comparison with the red line confirms the validity of the approximation. Other parameters are taken as $\kappa = 10 - 0.5i$, $N = 100$, $m_0 = 50$, and $h_z = 0.2$.

where $z = g/h_z$. Utilizing the multiplication theorem [71,73] for the Bessel function, we obtain

$$
\begin{aligned}
f_m^{(3)}(t) &= \Omega^{-1} \sum_n \frac{1}{n!} \left[\frac{ig \sin(2h_z t)}{h_z} \right]^n J_{m_0 - m + n}(x - g e^{-2ih_z t}/h_z) \\
&\approx \Omega^{-1} J_{m_0 - m}(x - g e^{-2ih_z t}/h_z) \\
&\quad + \Omega^{-1} \frac{ig \sin(2h_z t)}{h_z} J_{m_0 - m + 1}(x - g e^{-2ih_z t}/h_z),
\end{aligned}
\tag{28}
$$

under the condition of $|g| < h_z$.

While the results in Eqs. (27) and (28) indicate that this is a periodic oscillation with period $T = \pi/h_z$, the pattern is not so explicit. Nevertheless, for a finite system size N, we introduce the center of the wave packet:

$$
\mathcal{M}(t) = \frac{\sum_m m \left| f_m^{(3)}(t) \right|^2}{\sqrt{\sum_m \left| f_m^{(3)}(t) \right|^2}}.
\tag{29}
$$

The numerical results of $\mathcal{M}(t)$ for different values of g are presented in Fig. 3. The figure shows that the center of the wave packet undergoes the BO over time, and the amplitude is on the order of magnitude $|\kappa|$ for an imaginary g. However, for a real g, the center of the wave packet remains near the initial position m_0. This is opposite to that in the previous Gaussian initial state.

IV. NUMERICAL SIMULATIONS

Thus far, we have analyzed the time evolutions for three different initial excitations in the framework of the low-energy effective Hamiltonian in Eq (7). It is worth noting that in the non-Hermitian system, the magnetic BO is absent for an initial Gaussian state but emerges for an initial Bessel state, which is distinct from the Hermitian system. In this section, we present the numerical simulations of the time evolutions for the three initial states under the original Hamiltonian in Eq. (1), in order to verify the previous analyses.

The initial states are taken as

$$
|\Psi(0)\rangle = \sum_m f_m^{(n)}(0) \prod_{l \leqslant m} \sigma_l^- |\Uparrow\rangle
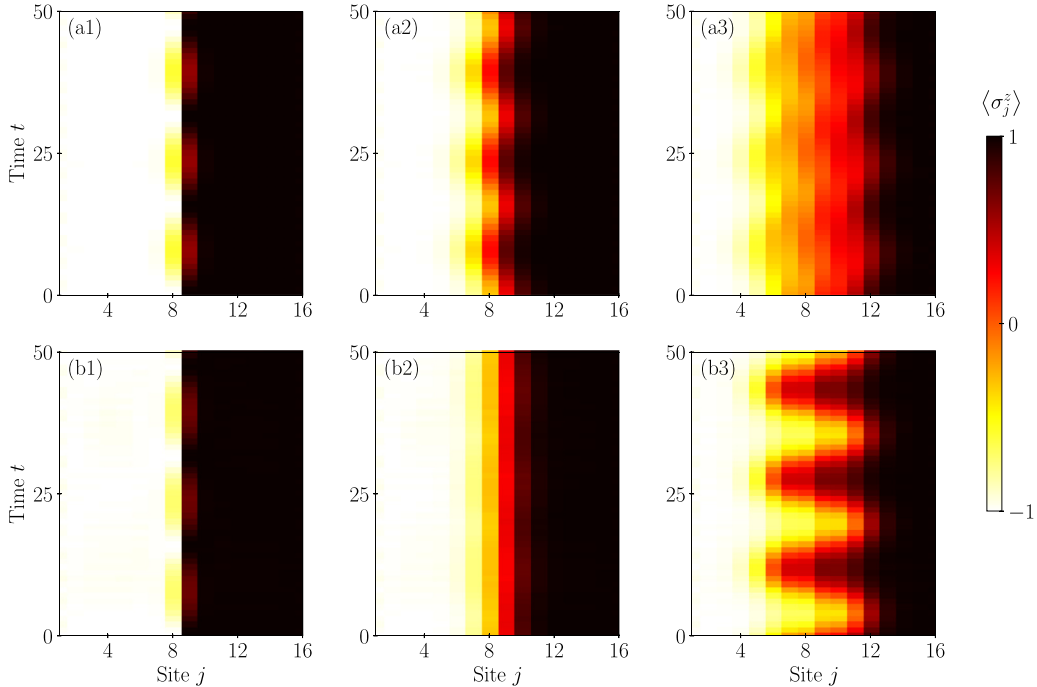\tag{30}
$$

FIG. 4. Numerical simulations of the time evolutions for the three different initial states in the (a1)–(a3) Hermitian spin chain with $g = 0.1$ and (b1)–(b3) non-Hermitian spin chain with $g = 0.1i$. In each figure, the expectation values of local spin σ_j^z as functions of time are presented. The initial states in the left, middle, and right panels are taken as the Kronecker delta state, Gaussian state with $\alpha = 0.4$ and $k_0 = 0$, and Bessel state with $\kappa = 4 - 0.5i$, respectively. Other parameters of the system: $N = 16$, $J = 1$, and $h_z = 0.2$.
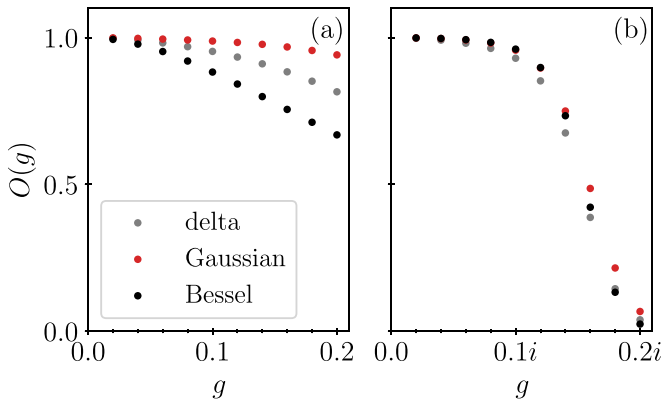
FIG. 5. Overlap of perturbative solutions and numerically evolved states at instant $t = 10$ for three different initial states considered in the main text. (a) Overlap for the Hermitian system as a function of real transverse field g. (b) Overlap for the non-Hermitian system as a function of imaginary transverse field g. Parameters of initial states are taken as the same as those in Fig. 4. Other parameters of the system are set as $N = 16$, $J = 1$, and $h_z = 0.2$.

with $n = 1$, 2, and 3, representing the Kronecker delta state, Gaussian state, and Bessel state, respectively, which are investigated in the previous section. The centers of these localized initial states are all set as $m_0 = 8$, i.e., at the middle of the chain, to avoid boundary effects. The evolved state $|\Psi(t)\rangle = e^{-iHt}|\Psi(0)\rangle/|e^{-iHt}|\Psi(0)\rangle|$ is calculated under the spin Hamiltonian in Eq. (1) using the fourth-order Runge-Kutta method with 5000 time steps of length $\Delta t = 0.01$, with a total accumulated error on the order of $O(\Delta t^4)$. The evolved state is normalized after each time step, and the local spin expectation value $\langle \sigma_j^z \rangle = \langle \Psi(t)|\sigma_j^z|\Psi(t)\rangle$ is computed after each 100 time steps. The results are presented in Fig. 4, and other parameters of the system and initial states are presented in the caption.

The boundary of $\langle \sigma_j^z \rangle = +1$ and -1 is the position of the magnetic domain wall. For the Hermitian spin chain, Figs. 4(a1)–4(a3) show that the dynamics are magnetic Bloch breathing, BO and stationary modes for the Kronecker delta, and Gaussian and Bessel initial states, respectively. With the same initial states, for the non-Hermitian spin chain, the results in Figs. 4(b1)–4(b3) indicate that the dynamics are magnetic Bloch breathing, stationary, and BO modes, respectively. For the latter two initial states, the corresponding BOs exhibit totally different patterns for the same initial states in the two different systems. These numerical results are in accordance with the analyses in the previous section.

In order to further estimate the validity of perturbative solutions presented in the previous section, we compare the numerical evolved states with perturbative solutions by the overlap

$$O = |\langle \Psi_{\text{num.}}(t)|\Psi_{\text{ana.}}(t)\rangle| \qquad (31)$$

at instant t, where $|\Psi_{\text{num.}}(t)\rangle$ and $|\Psi_{\text{ana.}}(t)\rangle$ denote the normalized numerical and analytical evolved states, respectively. The perturbative solutions $|\Psi_{\text{ana.}}(t)\rangle$ for three initial states are taken as the form of Eq. (16) with $f_m(t)$ being Eqs. (19), (23), and (27), respectively. In Fig. 5, we presented the numerical results of overlap O at instant $t = 10$ as a function of real and imaginary g. It indicates that for both cases, the perturbative solutions are in good agreement with the exact numerical results in a small $|g|$, while for imaginary g the overlap drops sharply when $|g| \gtrsim h_z/2 = 0.1$ due to the $\mathcal{PT}$ symmetry breaking of H that is not captured by the effective Hamiltonian H_{eff}.

V. SUMMARY

In summary, we demonstrate the existence of the magnetic BOs in a non-Hermitian quantum Ising chain. It is shown that in the small-field region, the low-energy dynamics of the magnetic domain walls are captured by a single-particle effective Hamiltonian, with the transverse field acting as a hopping coefficient for the magnetic domain wall and the strength of the longitudinal field playing the role of a skew potential. For real and imaginary transverse fields, the eigenstates of the effective Hamiltonian are both localized states with equally spaced energy levels, forming the WS ladders. Analytical and numerical calculations of the time evolution for the non-Hermitian quantum Ising chain show the following.

(i) The dynamics of the Kronecker delta initial state follow a breathing mode.

(ii) The Gaussian state remains stationary, which is different from the oscillation of the domain wall in a Hermitian quantum Ising chain.

(iii) For the Bessel initial state, the oscillation mode appears, and the amplitude can be modulated by the strength of the imaginary transverse field and the localization length of the initial state.

The validity of perturbative solutions is estimated by comparing them with numerical results. Our results reveal the mechanism of magnetic BOs in the non-Hermitian quantum spin chain and pave the way for future research on BOs in other quantum systems.

[1] F. Bloch, Über die quantenmechanik der elektronen in kristallgittern, Z. Phys. **52**, 555 (1929).

[2] C. Zener, A theory of the electrical breakdown of solid dielectrics, Proc. R. Soc. A **145**, 523 (1934).

[3] G. H. Wannier, Wave functions and effective hamiltonian for Bloch electrons in an electric field, Phys. Rev. **117**, 432 (1960).

[4] C. Waschke, H. G. Roskos, R. Schwedler, K. Leo, H. Kurz, and K. Köhler, Coherent submillimeter-wave emission from Bloch oscillations in a semiconductor superlattice, Phys. Rev. Lett. **70**, 3319 (1993).

[5] M. Ben Dahan, E. Peik, J. Reichel, Y. Castin, and C. Salomon, Bloch oscillations of atoms in an optical potential, Phys. Rev. Lett. **76**, 4508 (1996).

[6] S. R. Wilkinson, C. F. Bharucha, K. W. Madison, Q. Niu, and M. G. Raizen, Observation of atomic wannier-stark ladders in an accelerating optical potential, Phys. Rev. Lett. **76**, 4512 (1996).

[7] B. P. Anderson and M. A. Kasevich, Macroscopic quantum interference from atomic tunnel arrays, Science **282**, 1686 (1998).

[8] O. Morsch, J. H. Müller, M. Cristiani, D. Ciampini, and E. Arimondo, Bloch oscillations and mean-field effects of bose-einstein condensates in 1D optical lattices, Phys. Rev. Lett. **87**, 140402 (2001).

[9] R. Morandotti, U. Peschel, J. S. Aitchison, H. S. Eisenberg, and Y. Silberberg, Experimental observation of linear and nonlinear optical Bloch oscillations, Phys. Rev. Lett. **83**, 4756 (1999).

[10] H. Sanchis-Alepuz, Y. A. Kosevich, and J. Sánchez-Dehesa, Acoustic analogue of electronic Bloch oscillations and resonant Zener tunneling in ultrasonic superlattices, Phys. Rev. Lett. **98**, 134301 (2007).

[11] F. Meinert, M. Knap, E. Kirilov, K. Jag-Lauber, M. B. Zvonarev, E. Demler, and H.-C. Nägerl, Bloch oscillations in the absence of a lattice, Science **356**, 945 (2017).

[12] W. Zhang, H. Yuan, H. Wang, F. Di, N. Sun, X. Zheng, H. Sun, and X. Zhang, Observation of Bloch oscillations dominated by effective anyonic particle statistics, Nat. Commun. **13**, 2392 (2022).

[13] U. B. Hansen, O. F. Syljuåsen, J. Jensen, T. K. Schäffer, C. R. Andersen, M. Boehm, J. A. Rodriguez-Rivera, N. B. Christensen, and K. Lefmann, Magnetic Bloch oscillations and domain wall dynamics in a near-Ising ferromagnetic chain, Nat. Commun. **13**, 2547 (2022).

[14] J. Kyriakidis and D. Loss, Bloch oscillations of magnetic solitons in anisotropic spin-$\frac{1}{2}$ chains, Phys. Rev. B **58**, 5568 (1998).

[15] M. Sudzius, V. G. Lyssenko, F. Löser, K. Leo, M. M. Dignam, and K. Köhler, Optical control of Bloch-oscillation amplitudes: From harmonic spatial motion to breathing modes, Phys. Rev. B **57**, R12693 (1998).

[16] Y. A. Kosevich, Anomalous hall velocity, transient weak supercurrent, and coherent Meissner effect in semiconductor superlattices, Phys. Rev. B **63**, 205313 (2001).

[17] Z. Cai, L. Wang, X. C. Xie, U. Schollwöck, X. R. Wang, M. Di Ventra, and Y. Wang, Quantum spinon oscillations in a finite one-dimensional transverse Ising model, Phys. Rev. B **83**, 155119 (2011).

[18] S. Shinkevich and O. F. Syljuåsen, Spectral signatures of magnetic Bloch oscillations in one-dimensional easy-axis ferromagnets, Phys. Rev. B **85**, 104408 (2012).

[19] Y. A. Kosevich and V. V. Gann, Magnon localization and Bloch oscillations in finite Heisenberg spin chains in an inhomogeneous magnetic field, J. Phys.: Condens. Matter **25**, 246002 (2013).

[20] S. Shinkevich and O. F. Syljuåsen, Numerical simulations of laser-excited magnetic Bloch oscillations, Phys. Rev. B **87**, 060401(R) (2013).

[21] O. F. Syljuåsen, Dynamical structure factor of magnetic Bloch oscillations at finite temperatures, Eur. Phys. J. B **88**, 252 (2015).

[22] S. Longhi, Bloch oscillations in complex crystals with $\mathcal{PT}$ symmetry, Phys. Rev. Lett. **103**, 123601 (2009).

[23] L. Jin and Z. Song, Physics counterpart of the $\mathcal{PT}$ non-Hermitian tight-binding chain, Phys. Rev. A **81**, 032109 (2010).

[24] T. E. Lee and C.-K. Chan, Heralded magnetism in non-Hermitian atomic systems, Phys. Rev. X **4**, 041001 (2014).

[25] L. Jin, Topological phases and edge states in a non-Hermitian trimerized optical lattice, Phys. Rev. A **96**, 032103 (2017).

[26] C. Qin, B. Wang, Z. J. Wong, S. Longhi, and P. Lu, Discrete diffraction and Bloch oscillations in non-Hermitian frequency lattices induced by complex photonic gauge fields, Phys. Rev. B **101**, 064303 (2020).

[27] Y. Ashida, Z. Gong, and M. Ueda, Non-Hermitian physics, Adv. Phys. **69**, 249 (2020).

[28] L. Jin and Z. Song, Symmetry-protected scattering in non-Hermitian linear systems, Chin. Phys. Lett. **38**, 024202 (2021).

[29] W. Zhang, X. Ouyang, X. Huang, X. Wang, H. Zhang, Y. Yu, X. Chang, Y. Liu, D.-L. Deng, and L.-M. Duan, Observation of non-Hermitian topology with nonunitary dynamics of solid-state spins, Phys. Rev. Lett. **127**, 090501 (2021).

[30] J. Rohn, K. P. Schmidt, and C. Genes, Classical phase synchronization in dissipative non-Hermitian coupled systems, Phys. Rev. A **108**, 023721 (2023).

[31] C. Liang, Y. Tang, A.-N. Xu, and Y.-C. Liu, Observation of exceptional points in thermal atomic ensembles, Phys. Rev. Lett. **130**, 263601 (2023).

[32] H. S. Xu and L. Jin, Pseudo-Hermiticity protects the energy-difference conservation in the scattering, Phys. Rev. Res. **5**, L042005 (2023).

[33] H. S. Xu, L. C. Xie, and L. Jin, High-order spectral singularity, Phys. Rev. A **107**, 062209 (2023).

[34] S. Longhi, Dynamic localization and transport in complex crystals, Phys. Rev. B **80**, 235102 (2009).

[35] J. Ramya Parkavi, V. K. Chandrasekar, and M. Lakshmanan, Stable Bloch oscillations and landau-Zener tunneling in a non-Hermitian $\mathcal{PT}$-symmetric flat-band lattice, Phys. Rev. A **103**, 023721 (2021).

[36] S. Longhi, Exceptional points and Bloch oscillations in non-Hermitian lattices with unidirectional hopping, Europhys. Lett. **106**, 34001 (2014).

[37] S. Longhi, Bloch oscillations in non-Hermitian lattices with trajectories in the complex plane, Phys. Rev. A **92**, 042116 (2015).

[38] E.-M. Graefe, H. Korsch, and A. Rush, Quasiclassical analysis of Bloch oscillations in non-Hermitian tight-binding lattices, New J. Phys. **18**, 075009 (2016).

[39] M. Naghiloo, M. Abbasi, Y. N. Joglekar, and K. Murch, Quantum state tomography across the exceptional point in a single dissipative qubit, Nat. Phys. **15**, 1232 (2019).

[40] M. Partanen, J. Goetz, K. Y. Tan, K. Kohvakka, V. Sevriuk, R. E. Lake, R. Kokkoniemi, J. Ikonen, D. Hazra, A. Mäkinen, E. Hyyppä, L. Grönberg, V. Vesterinen, M. Silveri, and M. Möttönen, Exceptional points in tunable superconducting resonators, Phys. Rev. B **100**, 134505 (2019).

[41] Y. Wu, W. Liu, J. Geng, X. Song, X. Ye, C.-K. Duan, X. Rong, and J. Du, Observation of parity-time symmetry breaking in a single-spin system, Science **364**, 878 (2019).

[42] J. Li, A. K. Harter, J. Liu, L. de Melo, Y. N. Joglekar, and L. Luo, Observation of parity-time symmetry breaking transitions in a dissipative Floquet system of ultracold atoms, Nat. Commun. **10**, 855 (2019).

[43] Z. Ren, D. Liu, E. Zhao, C. He, K. K. Pak, J. Li, and G.-B. Jo, Chiral control of quantum states in non-Hermitian spin–orbit-coupled fermions, Nat. Phys. **18**, 385 (2022).

[44] K. L. Zhang and Z. Song, Ising chain with topological degeneracy induced by dissipation, Phys. Rev. B **101**, 245152 (2020).

[45] Y.-G. Liu, L. Xu, and Z. Li, Quantum phase transition in a non-Hermitian xy spin chain with global complex transverse field, J. Phys.: Condens. Matter **33**, 295401 (2021).

[46] K. L. Zhang and Z. Song, Quantum phase transition in a quantum Ising chain at nonzero temperatures, Phys. Rev. Lett. **126**, 116401 (2021).

[47] L. Lenke, M. Mühlhauser, and K. P. Schmidt, High-order series expansion of non-Hermitian quantum spin models, Phys. Rev. B **104**, 195137 (2021).

[48] N. Matsumoto, M. Nakagawa, and M. Ueda, Embedding the Yang-Lee quantum criticality in open quantum systems, Phys. Rev. Res. **4**, 033250 (2022).

[49] Z.-X. Guo, X.-J. Yu, X.-D. Hu, and Z. Li, Emergent phase transitions in a cluster Ising model with dissipation, Phys. Rev. A **105**, 053311 (2022).

[50] G. Sun, J.-C. Tang, and S.-P. Kou, Biorthogonal quantum criticality in non-Hermitian many-body systems, Front. Phys. **17**, 33502 (2022).

[51] H. Gao, K. Wang, L. Xiao, M. Nakagawa, N. Matsumoto, D. Qu, H. Lin, M. Ueda, and P. Xue, Experimental observation of the Yang-Lee quantum criticality in open systems, arXiv:2312.01706.

[52] C.-Z. Lu, X. Deng, S.-P. Kou, and G. Sun, Unconventional many-body phase transitions in a non-Hermitian Ising chain, arXiv:2311.11251.

[53] L. Lenke, A. Schellenberger, and K. P. Schmidt, Series expansions in closed and open quantum many-body systems with multiple quasiparticle types, Phys. Rev. A **108**, 013323 (2023).

[54] C. N. Yang and T. D. Lee, Statistical theory of equations of state and phase transitions. I. Theory of condensation, Phys. Rev. **87**, 404 (1952).

[55] T. D. Lee and C. N. Yang, Statistical theory of equations of state and phase transitions. II. Lattice gas and Ising model, Phys. Rev. **87**, 410 (1952).

[56] G. von Gehlen, Critical and off-critical conformal analysis of the Ising quantum chain in an imaginary field, J. Phys. A **24**, 5371 (1991).

[57] O. A. Castro-Alvaredo and A. Fring, A spin chain model with non-Hermitian interaction: The Ising quantum spin chain in an imaginary field, J. Phys. A **42**, 465211 (2009).

[58] N. Ananikian and R. Kenna, Imaginary magnetic fields in the real world, Physics **8**, 2 (2015).

[59] X. Peng, H. Zhou, B.-B. Wei, J. Cui, J. Du, and R.-B. Liu, Experimental observation of Lee-Yang zeros, Phys. Rev. Lett. **114**, 010601 (2015).

[60] T. Sanno, M. G. Yamada, T. Mizushima, and S. Fujimoto, Engineering Yang-Lee anyons via majorana bound states, Phys. Rev. B **106**, 174517 (2022).

[61] P. Pfeuty, The one-dimensional Ising model with a transverse field, Ann. Phys. (NY) **57**, 79 (1970).

[62] A. J. Daley, Quantum trajectories and open many-body quantum systems, Adv. Phys. **63**, 77 (2014).

[63] A. Biella and M. Schiró, Many-body quantum zeno effect and measurement-induced subradiance transition, Quantum **5**, 528 (2021).

[64] X. Turkeshi and M. Schiró, Entanglement and correlation spreading in non-Hermitian spin chains, Phys. Rev. B **107**, L020403 (2023).

[65] C. M. Bender and S. Boettcher, Real spectra in non-Hermitian Hamiltonians having $\mathcal{PT}$ symmetry, Phys. Rev. Lett. **80**, 5243 (1998).

[66] C. M. Bender, S. Boettcher, and P. N. Meisinger, $\mathcal{PT}$-symmetric quantum mechanics, J. Math. Phys. **40**, 2201 (1999).

[67] A. Mostafazadeh, Pseudo-Hermiticity versus PT symmetry: The necessary condition for the reality of the spectrum of a non-Hermitian Hamiltonian, J. Math. Phys. **43**, 205 (2002).

[68] M. Sanz, E. Solano, and Í. L. Egusquiza, Beyond adiabatic elimination: Effective Hamiltonians and singular perturbation, in *Applications + Practical Conceptualization+Mathematics= Fruitful Innovation: Proceedings of the Forum of Mathematics for Industry 2014* (Springer, New York, 2016), pp. 127–142.

[69] H. Fukuyama, R. A. Bari, and H. C. Fogedby, Tightly bound electrons in a uniform electric field, Phys. Rev. B **8**, 5579 (1973).

[70] D. O. Krimer, R. Khomeriki, and S. Flach, Delocalization and spreading in a nonlinear Stark ladder, Phys. Rev. E **80**, 036201 (2009).

[71] M. Abramowitz and I. A. Stegun, *Handbook of Mathematical Functions with Formulas, Graphs, and Mathematical Tables* (US GPO, Washington, DC, 1968), Vol. 55.

[72] M. Holthaus and D. W. Hone, Localization effects in ac-driven tight-binding lattices, Philos. Mag. B **74**, 105 (1996).

[73] C. Truesdell, On the addition and multiplication theorems for special functions, Proc. Natl. Acad. Sci. USA **36**, 752 (1950).